A SUPERVISED DYNAMIC LEARNING BACK-PROPAGATION (DLBP) NEURAL NETWORK APPROACH FOR AIRBORNE FULLY POLARIMETRIC SAR TARGET CLASSIFICATION

Associate Prof. Dr.-Ing. Jaan-Rong Tsay and M. Sc. Yih-Ling Lee
Department of Geomatics, National Cheng Kung University, No. 1, University Road, Tainan 701, TAIWAN; TEL: +886-6-2370876 ext. 838; email: tsayjr@mail.ncku.edu.tw

KEY WORDS: POLSAR, Target Classification, Neural Network, Back-Propagation

ABSTRACT: In this paper, we propose a supervised dynamic learning back-propagation (DLBP) classifier for target classification using airborne fully polarimetric SAR data. This approach is composed of a speckle noise filtering mechanism, fuzzy c-means approach, a non-linear scaling process of digital number for each dimension of feature space, and a dynamic learning back-propagation algorithm. The fuzzy approach is utilized to take mixed pixels or regions into account. A distance measure based on the complex Gaussian distribution has been applied to represent the distance between any two classes in the feature space. The proposed non-linear scaling operation could provide feature space data with both as higher signal-to-noise ratio as possible and with better separability between two classes. We use the NASA JPL fully polarimetric SAR (POLSAR) data in Taiwan for testing. The test results of the proposed DLBP are analyzed and compared with the minimum distance method. They show that separability measure might be better than SNR for defining the data scale for target classification. After changing the data scale, separability measures could raise 1.01~1.34 times than Lee filtered data. The accuracy of DLBP image classification is 89.37~94.40%.

1. INTRODUCTION

As a branch of geomatics, radargrammetry also aims at acquiring geometric, physical-radiometric and semantic data/information from microwave response signal in a as highly automatic manner as possible. For the purpose of acquisition of semantic data and information, different algorithms have been presented such as algorithms based on (1) image processing techniques, (2) statistical models, and (3) scattering mechanism of electromagnetic waves (Lee & Grunes, 1999; Chen et al., 2003). These algorithms can be either supervised or unsupervised. A number of classification algorithms attempt to derive and adopt effective feature vectors from polarizations for reducing data volume for SAR image classification. Leaving out the fully polarimetric information, only partial polarimetric information has been utilized. This does not necessarily mean that partial polarimetric data is not sufficient for the applications cited, but it does means that the full utilization of polarimetric data does seem to be necessary (Chen et al. 2003). This philosophy also guides us to develop the DLBP approach. (Chen et al. 2003) presents a supervised dynamic learning neural network (DLNN) classifier to use fully polarimetric information for SAR image classification. In this paper, the DLBP presents some news such logarithmic scaling process and a modified back-propagation algorithm.

2. A SUPERVISED DLBP APPROACH

Figure 1 illustrates briefly our supervised DLBP approach. More details are given in the following sections.

2.1 Input Original Polarimetric SAR Data

Figure 2 illustrates the main network configuration of the DLBP for utilizing the complete polarimetric SAR data inputs from multi-bands, e.g. C-, L- and P-band. The polarimetric data from the input layer are the elements of feature vector for a pixel, where $S_{hh}S_{hh}^{*} = |S_{hh}|^2$, $S_{hv}S_{hv}^{*} = |S_{hv}|^2$, $S_{vv}S_{vv}^{*} = |S_{vv}|^2$ are the diagonal entries in the polarimetric covariance matrix C and

$S_{hh}S_{vv}^*$, $S_{hv}S_{hh}^*$, $S_{vv}S_{hv}^*$ are the non-diagonal terms in C. The six non-diagonal elements in the polarimetric covariance matrix C can be reduced to three terms, because C is a Hermitian matrix. In general, all the non-diagonal terms $S_{hh}S_{vv}^*$, $S_{hv}S_{hh}^*$, $S_{vv}S_{hv}^*$ are complex values and are expressed as real and imagery parts denoted by R() and I() in Figure 2, respectively. The values in the output layer of neural network are the membership value α_{ci} of an interest pixel *i* to a certain class *c*.

Input original polarimetric SAR data
Polarimetric speckle filtering
Logarithmic scaling process of feature vector
DLBP training, if needed:
    Training pixels choosing
    Fuzzy c-means (FCM) clustering of training pixels
    Determining memberships of training pixels
    DLBP training
    Generating Weights of DLBP
DLBP classification:
    Input filtered polarimetric SAR image and weights of DLBP
    Iterative computation of DLBP classification
    Output memberships of SAR image
    Winner-take-all criterion
    Generating classification map

Figure 1. A supervised dynamic learning back-propagation (DLBP) classification approach

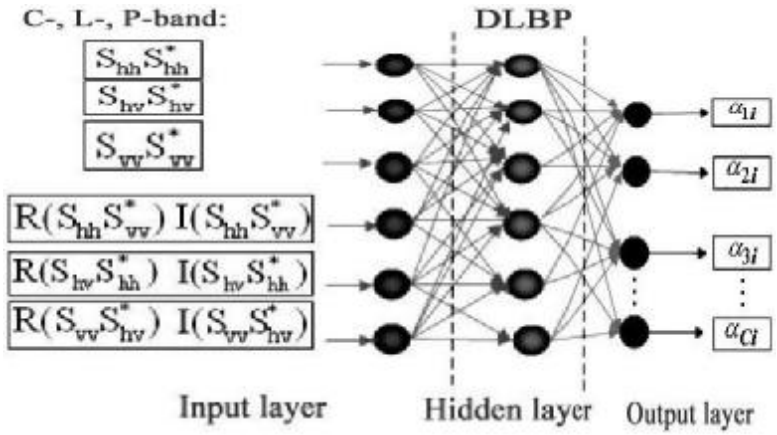

Figure 2. Input, hidden and output layers of the DLBP

2.2 Polarimetric Speckle Filtering

In order to increase SAR image quality, SAR images are often multilook processed by averaging several neighboring one-look pixels. This computation equation is as follows:

$$\nu = \frac{1}{n}\sum_{i=1}^{n} C_i \qquad (1)$$

where C_i is the one-look covariance matrix of the *i*-th pixel, and *n* is the number of looks. Thus, the ν statistics have a complex Wishart distribution (Goodman, 1963). A pixel in an SAR image is formed by the vector sum of echoes from all scatters within the illuminated cell. All scatters in that resolution cell may not be electromagnetically homogeneous and their geolocations in relation to the radar are random. A random walk phenomenon occurs that causes speckle noise (Chen et al. 2003). SAR image interpretation and classification suffers from this

speckle contamination. To further reduce the effect of speckle, (Lee et al., 1999) presented a polarimetric filter to avoid cross-talk, while preserving the edge sharpness and the polarimetric properties. Therefore, the DLBP approach adopts both multilook-averaging operation and Lee-filter for polarimetric speckle filtering process. The thus filtered SAR data are then the inputs to the DLBP classification.

2.3 Complex Wishart Distance Measure

In order to include complete fully polarimetric information, (Lee et al., 1994) defined a distance measure based on Wishart distribution. Without *a priori* information, an equal probability for each class is often assumed. This distance measure is then reduced to

$$d(\nu,\omega_m) = \ln|\omega_m| + Tr\left(\omega_m^{-1}\nu\right) \tag{2}$$

where ω_m is the cluster center of the covariance matrix for the *m*-th class, and Tr denotes the trace of a matrix.

2.4 Logarithmic Scaling Process

The digital numbers of inputs are in this step logarithmically scaled where not only the signal-to-noise ratio SNR should not be decreased, but also the separability measure SM between any two classes should be increased. The equation (3) is used to evaluate the SNR-value for each real dimension ($S_{hh}S_{hh}^*$, $S_{hv}S_{hv}^*$, $S_{vv}S_{vv}^*$), and equation (4) for each complex dimension ($S_{hh}S_{vv}^*$, $S_{hv}S_{hh}^*$, $S_{vv}S_{hv}^*$).

$$SNR = \frac{1}{MN}\sum_{y=1}^{M}\sum_{x=1}^{N}\sqrt{\frac{\sum_{i=1}^{3}\sum_{j=1}^{3}p_{ij}^2}{\sum_{i=1}^{3}\sum_{j=1}^{3}\left(p_{ij}-\bar{p}\right)^2}} \tag{3}$$

$$SNR = \frac{1}{MN}\sum_{y=1}^{M}\sum_{x=1}^{N}\sqrt{\frac{\sum_{i=1}^{3}\sum_{j=1}^{3}A_{ij}^2}{\sum_{i=1}^{3}\sum_{j=1}^{3}\left(A_{ij}-\bar{A}\right)^2}} \tag{4}$$

where $\bar{p}$ is the average of all real numbers p_{ij} in a 3x3 window, and the size of SAR image computed is M x N. $\bar{A}$ is the average amplitude of all complex numbers in a 3x3 window. Not to change any phase information, the scale of digital numbers is logarithmically changed (equation (5)) for real elements and amplitude components of complex elements in C.

$$\hat{z} = a \cdot \log_b z \tag{5}$$

where z denotes p_{ij} or A_{ij}. Also, the separability measure SM between the *i*-th and *j*-th class is defined by

$$\text{SM}=\frac{\left|\bar{p}_i-\bar{p}_j\right|}{\hat{\sigma}_i+\hat{\sigma}_j} \text{ for real elements;} \qquad \text{SM}=\frac{\sqrt{\left(\bar{a}_i-\bar{a}_j\right)^2+\left(\bar{b}_i-\bar{b}_j\right)^2}}{\hat{\sigma}_i+\hat{\sigma}_j} \text{ for complex element} \tag{6}$$

where $\bar{p}_i$, $\bar{p}_j$ are the averages of a certain real dimension for *i*-th and *j*-th class; $\bar{a}_i$, $\bar{a}_j$ are the averages of real parts of a certain complex dimension for *i*-th and *j*-th class; $\bar{b}_i$, $\bar{b}_j$ are the averages of imaginary parts of a certain complex dimension for *i*-th and *j*-th class; $\hat{\sigma}_i$, $\hat{\sigma}_j$ are

the standard deviations of all pixels for the *i*-th and *j*-th class from their cluster center, respectively. A set of optimal parameter values *a* and *b* in the equation (5) is then determined by numerical analysis, in which all available pixels with known ground truth are used.

2.5 A Fuzzy Back-Propagation Approach

This approach is composed of the following steps.

Step 1: Setting the configuration of neural network. The numbers *i*, *h*, *j* of neurons in input, hidden and output layers are defined. Learning rate η, momentum *m*, weights $\boldsymbol{w_{ih}}$, $\boldsymbol{w_{hj}}$, and bias $\boldsymbol{b_h}$, $\boldsymbol{b_j}$ are chosen. A fuzzy index Z=2 is used.

Step 2: Defining an initial weight vector $\boldsymbol{U} = \left[\mu_{ik}^{(0)}\right]$ by

$$\mu_{ik}^{(0)} = \left[\sum_{j=1}^{c} \left(\frac{\left\| \boldsymbol{x_k} - \boldsymbol{v_i^{(0)}} \right\|}{\left\| \boldsymbol{x_k} - \boldsymbol{v_j^{(0)}} \right\|} \right)^{\frac{2}{Z-1}} \right]^{-1} \quad \text{for } 1 \le i \le c \tag{7}$$

Step 3: Computing weight increments $\Delta \boldsymbol{w_{hj}}, \Delta \boldsymbol{w_{ih}}$ and bias increments $\Delta \boldsymbol{b_j}, \Delta \boldsymbol{b_h}$ by

$$\Delta w_{hj}(p+1) = \eta \delta_j H_h + m \Delta w_{hj}(p) \text{ and } \Delta b_j(p+1) = -\eta \delta_j + m \Delta b_j(p) \text{ for output layer;}$$
$$\Delta w_{ih}(p+1) = \eta \delta_h X_i + m \Delta w_{ih}(p) \text{ and } \Delta b_h(p+1) = -\eta \delta_h + m \Delta b_h(p) \text{ for hidden layer} \tag{8}$$

Step 4: Updating weight matrices $\boldsymbol{w_{hj}}, \boldsymbol{w_{ih}}$ and weight bias vectors $\boldsymbol{b_j}, \boldsymbol{b_h}$ by

$$w_{hj}(p+1) = w_{hj}(p) + \Delta w_{hj}(p) \text{ and } b_j(p+1) = b_j(p) + \Delta b_j(p) \text{ for input layer;}$$
$$w_{ih}(p+1) = w_{ih}(p) + \Delta w_{ih}(p) \text{ and } b_h(p+1) = b_h(p) + m \Delta b_h(p) \text{ for hidden layer} \tag{9}$$

Step 5: Computing the c-means vector by

$$\boldsymbol{v_i^{(p)}} = \frac{\sum_{k=1}^{n} \left(\mu_{ik}^{(p)} \right)^{Z} \boldsymbol{x_k}}{\sum_{k=1}^{n} \left(\mu_{ik}^{(p)} \right)^{Z}} \quad \text{for } 1 \le i \le c \tag{10}$$

$$\boldsymbol{U_{c \times n}^{(p+1)}} = \left[\mu_{cn}^{(p+1)} \right] = \begin{bmatrix} \mu_{11}^{(p+1)} & \mu_{12}^{(p+1)} & \cdots & \mu_{1n}^{(p+1)} \\ \mu_{21}^{(p+1)} & \mu_{22}^{(p+1)} & \cdots & \mu_{2n}^{(p+1)} \\ \vdots & \vdots & \ddots & \vdots \\ \mu_{c1}^{(p+1)} & \mu_{c2}^{(p+1)} & \cdots & \mu_{cn}^{(p+1)} \end{bmatrix} \text{ for the } p\text{-th iteration} \tag{11}$$

$$\mu_{ik}^{(p+1)} = \left[\sum_{j=1}^{c} \left(\frac{\boldsymbol{d}\left(\boldsymbol{x_k}, \boldsymbol{v_i^{(p)}} \right)}{\boldsymbol{d}\left(\boldsymbol{x_k}, \boldsymbol{v_j^{(p)}} \right)} \right)^{\frac{2}{Z-1}} \right]^{-1} \quad \text{for } 1 \le i \le c \tag{12}$$

Step 6: Repeat the steps 3~5 until the following two conditions hold:

$$\frac{1}{2} \sum_j \left(\boldsymbol{T_j} - \sum_i \boldsymbol{w_{ij}} \boldsymbol{x_i} \right)^{\boldsymbol{T}} \left(\boldsymbol{T_j} - \sum_i \boldsymbol{w_{ij}} \boldsymbol{x_i} \right) < \varepsilon \text{ and } \left\| \boldsymbol{U^{(p+1)}} - \boldsymbol{U^{(p)}} \right\| < \boldsymbol{t} \tag{13}$$

or until the maximal number of iterations is reached, where ε and *t* are two thresholds.

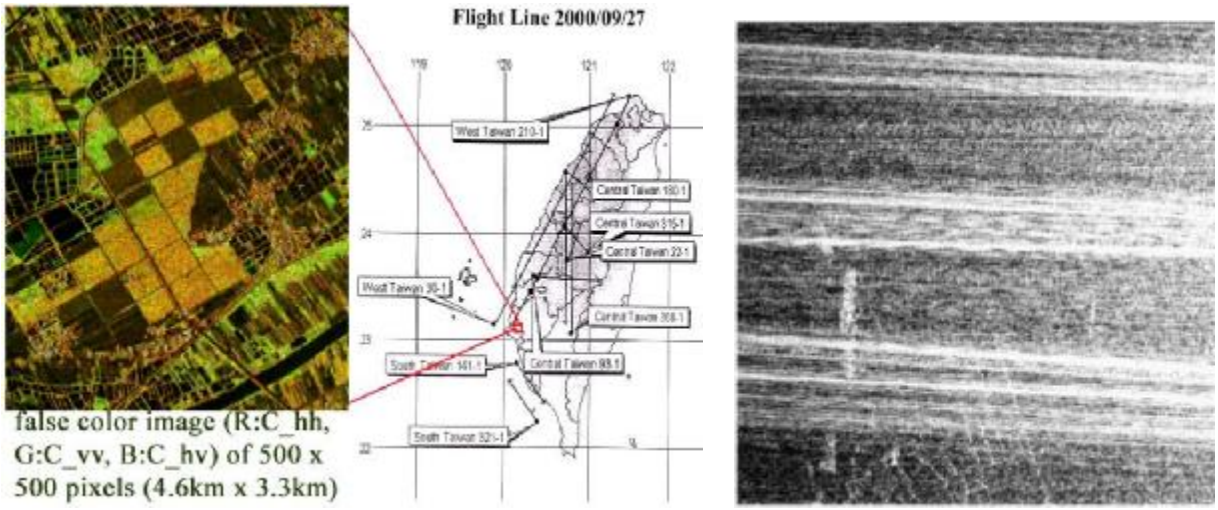

Figure 3. Test area in the south Taiwan (left) and a P_hh image of 580 x 600 pixels (right)

Figure 4. the ground truth data (left) and the chosen training pixels (right) in the test area, with (dry land), (road), (sugar cane) and (water body).

3. TEST RESULTS

Figure 3 shows the test area, which is flat farmland in the south Taiwan. The P-band data is not available, since apparent effect of a certain electric wave disturbance appears. Thus, only the fully polarimetric SAR images of C- and P-band are used. These data are acquired on September 27, 2000, during the 2000 Pacrim-II campaign. Figure 5 shows that C-band data has better SNR than L-band, and the filtering operation does improve the SAR image quality. Test results show that the separability measure SM is a better index than SNR for choosing an optimal logarithmic scale for representing digital number (DN) of each element in the polarimetric covariance matrix. The SM value of scaled DN-values is 1.01~1.34 times larger than filtered ones. The minimum-distance-to-means classifier has a overall accuracy of 89.93~96.41%, while the DLBP has a overall accuracy of 89.37%~94.40%. The filtered inputs provide an overall classification accuracy of 90.52~96.41%, while the original inputs only with multilook-averaged operation provide a worse overall accuracy of 89.37~90.46%. The Euclidean distance provides an overall accuracy of 89.37~96.41%, while the complex Wishart distance provides an overall accuracy of 89.54~91.08%.

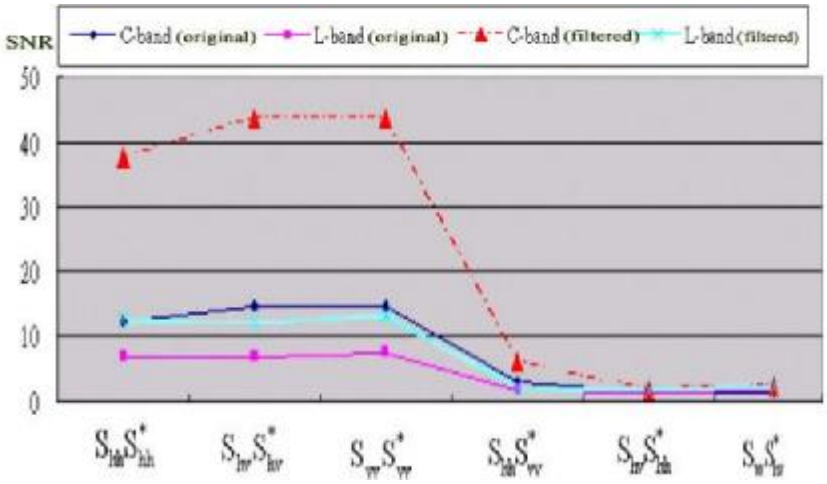

Figure 5. SNR values of original and filtered polarimetric SAR images

4. CONCLUSION AND FUTURE WORKS

This paper presents the DLBP classifier for fully polarimetric SAR image data, which integrates a fuzzy back-propagation neural network as a classifier, a scale regulator, a covariance matrix as a feature vector, and a distance measure based on a complex Wishart distribution, has been demonstrated. DLBP is capable of handling the mixed pixels. Also, the DLBP has a potential to include high level features, such as intrinsic features (e.g. shape, texture), topological features, context features, class relationship, and class inheritance relationship as well, to improve classification accuracy. It needs further study.

REFERENCE

Chen, C.-T., Chen, K.-S., and Lee, J.-S., 2003. The Use of Fully Polarimetric Information for the Fuzzy Neural Classification of SAR Images. IEEE Transactions on Geoscience and Remote Sensing, Vol. 41, No. 9, pp. 2089-2100.

Goodman, N.R., 1963. Statistical Analysis Based on a Certain Complex Gaussian distribution (an Introduction), Ann. Math. Statist., Vol. 34, pp. 152-177.

Lee, J.S., Grunes, M.R., and Kowk, R., 1994. Classification of Multi-Look Polarimetric SAR Imagery Based on Complex Wishart Distribution, International Journal of Remote Sensing, Vol. 15, No. 11, pp. 2299-2311.

Lee, J.S., and Grunes, M.R., 1999. Polarimetric SAR speckle filtering and terrain classification – an overview. In: Information Processing for Remote Sensing, edited by C.H. Chen, World Scientific, Singapore, pp. 113-138.

Lee, J.S., Grunes, M.R., and Grandi, G. de, 1999. Polarimetric SAR Speckle Filtering and its Implication for Classification, IEEE Transactions on Geoscience and Remote Sensing, Vol. 37, pp. 2363-2373.

ACKNOWLEDGEMENT

We greatly appreciate the NSC (=National Science Committee), TAIWAN, for sponsoring this work under the research project NSC 92-2211-E-006-093. Also, we wish to express our sincere gratitude Dr. Chia-Tang Chen and Prof. Dr. Kun-Shan Chen from the Center for Space and Remote Sensing Research, National Central University, Taiwan, for their great help in clarifying the concepts. Special thanks also go to Dr. Bruce Chapman from the Jet Propulsion Laboratory, NASA, USA, for his clarifying the POLSAR data format.